

## Article

# Structural and Theoretical Study of Copper(II)-5-fluoro Uracil Acetate Coordination Compounds: Single-Crystal to Single-Crystal Transformation as Possible Humidity Sensor

Verónica G. Vegas <sup>1</sup>, Andrea García-Hernán <sup>1</sup> , Fernando Aguilar-Galindo <sup>2</sup> , Josefina Perles <sup>3,\*</sup>   
and Pilar Amo-Ochoa <sup>1,4,\*</sup> 

- <sup>1</sup> Departamento de Química Inorgánica, Facultad de Ciencias, Universidad Autónoma de Madrid, 28049 Madrid, Spain; veronica.garciav@estudiante.uam.es (V.G.V.); andrea.garciah@uam.es (A.G.-H.)  
<sup>2</sup> Departamento de Química, Facultad de Ciencias, Universidad Autónoma de Madrid, 28049 Madrid, Spain; fernando.aguilar-galindo@uam.es  
<sup>3</sup> Laboratorio de DRX Monocristal, Servicio Interdepartamental de Investigación, Universidad Autónoma de Madrid, 28049 Madrid, Spain  
<sup>4</sup> Institute for Advanced Research in Chemical Sciences (IAdChem), Universidad Autónoma de Madrid, 28049 Madrid, Spain  
\* Correspondence: josefina.perles@uam.es (J.P.); pilar.amo@uam.es (P.A.-O.)



**Citation:** Vegas, V.G.; García-Hernán, A.; Aguilar-Galindo, F.; Perles, J.; Amo-Ochoa, P. Structural and Theoretical Study of Copper(II)-5-fluoro Uracil Acetate Coordination Compounds: Single-Crystal to Single-Crystal Transformation as Possible Humidity Sensor. *Polymers* **2023**, *15*, 2827. <https://doi.org/10.3390/polym15132827>

Academic Editor: Beatriz Gil-Hernández

Received: 27 April 2023

Revised: 13 June 2023

Accepted: 19 June 2023

Published: 26 June 2023



**Copyright:** © 2023 by the authors. Licensee MDPI, Basel, Switzerland. This article is an open access article distributed under the terms and conditions of the Creative Commons Attribution (CC BY) license (<https://creativecommons.org/licenses/by/4.0/>).

**Abstract:** This paper describes the synthesis and characterization of seven different copper(II) coordination compounds, as well as the formation of a protonated ligand involving all compounds from the same reaction. Their synthesis required hydrothermal conditions, causing the partial in situ transformation of 5-fluoro uracil-1-acetic acid (5-FUA) into an oxalate ion (ox), as well as the protonation of the 4,4'-bipyridine (bipy) ligand through a catalytic process resulting from the presence of Cu(II) within the reaction. These initial conditions allowed obtaining the new coordination compounds  $[\text{Cu}_2(5\text{-FUA})_2(\text{ox})(\text{bipy})]_n \cdot 2n \text{ H}_2\text{O}$  (CP2),  $[\text{Cu}(5\text{-FUA})_2(\text{H}_2\text{O})(\text{bipy})]_n \cdot 2n \text{ H}_2\text{O}$  (CP3), as well as the ionic pair  $[(\text{H}_2\text{bipy})^{+2} 2\text{NO}_3^-]$  (1). The mother liquor evolved rapidly at room temperature and atmospheric pressure, due to the change in concentration of the initial reagents and the presence of the new chemical species generated in the reaction process, yielding CPs  $[\text{Cu}(5\text{-FUA})_2(\text{bipy})]_n \cdot 3.5n \text{ H}_2\text{O}$ ,  $[\text{Cu}_3(\text{ox})_3(\text{bipy})_4]_n$  and  $[\text{Cu}(\text{ox})(\text{bipy})]_n$ . The molecular compound  $[\text{Cu}(5\text{-FUA})_2(\text{H}_2\text{O})_4] \cdot 4\text{H}_2\text{O}$  (more thermodynamically stable) ended up in the mother liquor after filtration at longer reaction times at 25 °C and 1 atm., cohabiting in the medium with the other crystalline solids in different proportions. In addition, the evaporation of  $\text{H}_2\text{O}$  caused the single-crystal to single-crystal transformation (SCSC) of  $[\text{Cu}(5\text{-FUA})_2(\text{H}_2\text{O})(\text{bipy})]_n \cdot 2n \text{ H}_2\text{O}$  (CP3) into  $[\text{Cu}(5\text{-FUA})_2(\text{bipy})]_n \cdot 2n \text{ H}_2\text{O}$  (CP4). A theoretical study was performed to analyze the thermodynamic stability of the phases. The observed SCSC transformation also involved a perceptible color change, highlighting this compound as a possible water sensor.

**Keywords:** copper; humidity sensors; coordination compounds; coordination polymers; theoretical calculations

## 1. Introduction

Coordination compounds (CCs) are formed by the self-assembly of several building blocks (usually metal ions and organic ligands) and have been known for more than 100 years [1]. Their research has not stopped growing in different fields (porous materials, cancer, bioimaging, photocatalysis, etc.) [2–5], with more than 10,000 annual publications in the last decade (Web of Science). They are usually obtained via direct synthesis in a single step, often under mild conditions [2,6,7].

The search for infinite structures (coordination polymers or CPs) is a subarea within CCs that has been of great interest, e.g., in the obtention of new semiconductor materials

with selective molecular recognition or porous CPs (metal–organic frameworks, MOFs), among others [8–13].

These infinite structures are usually insoluble, and this aspect has hindered their structural characterization [14]. For this reason, the synthetic conditions have been modified using new synthesis routes under more extreme conditions (solvothermal synthesis) that facilitate the formation of quality crystals for their subsequent resolution via single-crystal X-ray diffraction [15]. The solvothermal reactions have, in turn, favored new unconventional coordination environments [16], in situ ligand transformations, redox processes of the metal center [17], and even reactions catalyzed by the presence of the metal ion [18], among others. The behavior of CCs under high pressure and temperature is an amazing research area that allows the creation of new materials with interesting properties [16,19,20].

On the other hand, a fundamental characteristic of CCs is that their bond is highly dynamic, which makes these materials very versatile since they respond to different stimuli [21–23]. The lability of the bonds allows interesting structural modifications in the same reaction medium, as a consequence of small differences in the medium temperature, or the reagents concentrations, among others [24]. These transformations can sometimes maintain the single-crystal structural integrity during the modification (single-crystal to single-crystal or SCSC transformations) and are also a very interesting source of knowledge [25,26].

SCSC transformations, in the case of CCs, are also favored by the lability of the coordination bond and are controlled by various factors such as the coordination preference of the metal ion. There are several types of external physical and chemical factors that favor or induce these transformations, such as light, pressure, cooling, heating [27,28], or the presence of gases [29]. Generally, the variations between the two structural types must be small; for example, the presence of gases can cause molecular substitution in the coordination environment of the metal center [30]. The breaking and rearrangement as a result of the new bond will change the crystalline structure of the final compound and, therefore, its properties [30].

For these reasons, the study of the structural modifications in the reaction medium is key and essential to understand the CC behavior, e.g., from the biochemical point of view (important in their possible use as pharmaceuticals or drug delivery) [31] or can be used in the design of new compounds with the desired properties. Indeed, SCSC studies may have applications in the manufacture of sensors, gas storage, etc.

In this sense, the study of low-cost humidity sensors, with easy handling (visual change) and high durability, is always desirable [32,33] and often essential in areas such as civil engineering and construction materials where it is important to determine the safety, reliability, and service life of large-scale public infrastructure highly sensitive to moisture and environmental factors that damage building structures [34]. The use of sensors will allow controlling their deterioration [35].

Along with technological advancements, many types of sensors have been used in construction engineering to provide a wide variety of data for management and maintenance. Currently, they are mostly applied to monitor indoor environments in order to enable comfortable environment management [36]. Indeed, according to McMullan [37], relative humidity should be kept between 30% and 70% to achieve thermal comfort and avoid condensation risks.

Therefore, in this work, in addition to the obtention, isolation, and characterization of eight different compounds starting from the same hydrothermal synthesis conditions using Cu(II), 4,4'-bipyridine (bipy), and 5-fluorouracil-1-acetic acid (5-FUA) as building blocks, a perceptible color change as a result of an SCSC transformation is also observed. This transformation is initiated by the decrease of water in the environment; consequently, taking advantage of this physical property, we study its possible behavior as a colorimetric humidity sensor. Additionally, we use theoretical calculations to understand the SCSC transformation observed.

## 2. Materials and Methods

All reagents and solvents were purchased from standard chemical suppliers and used as received:  $\text{Cu}(\text{NO}_3)_2 \cdot 3\text{H}_2\text{O}$  extra pure Scharlab (Barcelona, Spain) (CAS: 10031-43-3) and 4,4'-bipyridine 98%, ACROS Organics (Madrid, Spain) (CAS: 553-26-4), 5-fluorouracil 98%, ACROS Organics (Madrid, Spain) (CAS: 38771-21-1), and chloroacetic acid 99+% (CAS: 79-11-8). The synthesis of the 5-fluorouracil-1-acetic acid was performed in line with previous work [38].

**Infrared (FT-IR)** spectra were recorded on a PerkinElmer (Madrid, Spain) model 100 spectrophotometer using a PIKE (Cottonwood, WI, USA) Technologies MIRacle Single-Reflection Horizontal ATR Accessory from 4000–500  $\text{cm}^{-1}$ .

**Elemental analysis** was performed on an elementary microanalyzer LECO (Madrid, Spain) CHNS-932. It works with controlled doses of  $\text{O}_2$  and a combustion temperature of 1000 °C.

**Powder X-ray diffraction (PXRD)** were collected using a PANalytical (Malvern, UK) X'Pert PRO MPD  $\theta/2\theta$  secondary monochromator and detector with fast X'Celerator, which was used for general assays. The samples were analyzed with  $\theta/2\theta$  scanning. Theoretical X-ray powder diffraction patterns were calculated using Mercury software version 4.0.0 from the Crystallographic Cambridge Database Center (Cambridge, UK).

**Single-crystal X-ray diffraction (SCXRD)** was performed on suitable single crystals, which were isolated, coated with mineral oil, and mounted on MiTeGen Micro-Mounts (Ithaca, NY, USA). The samples were measured in a Bruker (Madison, WI, USA) D8 Kappa diffractometer (with APEX II area-detector system, equipped with graphite monochromated  $\text{Mo K}\alpha$  radiation ( $\lambda = 0.71073 \text{ \AA}$ ). The substantial redundancy in data allowed empirical absorption corrections [39] to be applied using multiple measurements of symmetry-equivalent reflections. Raw intensity data frames were integrated with the SAINT [40] program, which was also used to apply corrections for Lorentz and polarization effects. The Bruker SHELXTL Software Package [41] was used for space group determination, structure solution, and refinement. The space group determination was based on a check of the Laue symmetry, and systematic absences were confirmed using the structure solution. The structures were solved by direct methods [42] completed with different Fourier syntheses and refined with full-matrix least-squares minimizing  $w(F_o^2 - F_c^2)^2$ . Weighted R factors ( $wR$ ) and all goodness of fit  $S$  were based on  $F^2$ ; conventional R factors ( $R$ ) were based on  $F$ . All scattering factors and anomalous dispersion factors were contained in the SHELXTL 6.10 program library. All non-hydrogen atoms were refined with anisotropic displacement parameters. Hydrogen atoms were placed at calculated positions except the ones from water molecules included in the models, which were located in the electron density maps.

The crystal structures of the compounds  $[(\text{H}_2\text{bipy})^{+2} 2\text{NO}_3^-]$  (**1**), **CP2**, **CP3**, and **CP4** were deposited in the CSD (<https://www.ccdc.cam.ac.uk>, accessed on 18 June 2023) with CCDC numbers 2243124, 2243125, 2243126, and 2243127, respectively; they can be retrieved free of charge from the Cambridge Crystallographic Data Center via [www.ccdc.cam.ac.uk/data\\_request/cif](http://www.ccdc.cam.ac.uk/data_request/cif) (accessed on 18 June 2023) (Figures S10–S14 and Tables S1–S11).

**Synthesis of  $[(\text{H}_2\text{bipy})^{+2} 2\text{NO}_3^-]$  (**1**),  $[\text{Cu}_2(5\text{-FUA})_2(\text{ox})(\text{bipy})]_n \cdot 2n \text{H}_2\text{O}$  (**CP2**),  $[\text{Cu}(5\text{-FUA})_2(\text{H}_2\text{O})(\text{bipy})]_n \cdot 2n \text{H}_2\text{O}$  (**CP3**)**

5-Fluorouracil-1-acetic acid (**5-FUA**) (75.5 mg, 0.41 mmol),  $\text{Cu}(\text{NO}_3)_2 \cdot 3\text{H}_2\text{O}$  (54.6 mg, 0.205 mmol), and bipy (0.125 g, 0.8 mmol) were mixed in 9 mL of MilliQ water ( $\text{pH}_i = 2.3$ ) in a glass hydrothermal (25 mL) reactor and magnetically stirred (900 rpm) for 10 min at room temperature. During this time, a color change from light to dark blue was observed. Then, the mixture was heated at 120 °C for 48 h, followed by a cooling ramp at ca. 0.066 °C/min. After that ( $\text{pH}_f = 2.75$ ), a mixture of compounds **CP2**, **CP3**, and **1** (Figure S1, see in Supplementary Materials) in different proportions was obtained. The mixture was filtered off and manually separated under optical microscopy. Turquoise crystals (**CP2**) were suitable for single-crystal X-ray diffraction studies (Figure S10 and Tables S3 and S4), (75% yield based on Cu). Analytically calculated (found) for  $\text{C}_{12}\text{H}_{13}\text{CuFN}_3\text{O}_9$ : C, 37.1%

(36.8%); H, 2.1% (2.3%); N, 10.9% (10.5%). Characteristic IR bands ( $\text{cm}^{-1}$ ): 3065 (w), 1672(s), 1595 (s), 1400 (m), 1372 (m), 1242 (m) 1076 (w), 985 (m), and 824 (m) (Figure S5). Blue crystals suitable for single-crystal X-ray diffraction studies of **CP3** (Figure S11) were also isolated (yield 3% based on Cu). Characteristic IR bands ( $\text{cm}^{-1}$ ): 3460 (w), 1698 (s), 1600 (s), 1407 (m), 1302 (m), 1236 (s), and 823 (w). Yellow crystals suitable for single-crystal X-ray diffraction studies ( $[(\text{H}_2\text{bipy})^{+2} 2.\text{NO}_3^-]$  (**1**)) (Figure S9) were also isolated (yield 7% based on Cu). Characteristic IR bands ( $\text{cm}^{-1}$ ): 3062 (m), 2938 (w), 1720 (w), 1641 (s), 1430 (s), 1347 (m), 1239 (s), 867 (m), and 806 (s) (Figure S4).

#### Single-crystal to single-crystal transformation of compound $[\text{Cu}(\text{5-FUA})_2(\text{H}_2\text{O})(\text{bipy})]_n \cdot 2n \text{H}_2\text{O}$ (**CP3**) into $[\text{Cu}(\text{5-FUA})_2(\text{bipy})]_n \cdot 2n \text{H}_2\text{O}$ (**CP4**)

Once compound **CP3** was separated from the mother liquor in ambient conditions, a color change from dark blue to violet occurred, indicative of a single-crystal to single-crystal transformation. The resulting crystals, with formula **CP4** were suitable for single-crystal X-ray diffraction structure solution (Figure S12). Analytically calculated (found) for  $\text{C}_{11}\text{H}_{10}\text{Cu}_{0.5}\text{FN}_3\text{O}_5$ : C, 40.8% (41.1%); H, 3.4% (2.9%); N, 12.9% (12.6%).

#### Humidity sensor study

To measure the percentage of moisture at which the violet compound **CP4** changed its color reversibly to blue **CP3**, crystals of the former compound, together with a hygrometer, were placed into a dry box with an initial environmental humidity percentage between 25% and 35% (the experiment was carried out three times to ensure reproducibility). Inside the dry box, a beaker with water on a heating plate was also placed to increase the environmental humidity, observing the change in color to blue at 70% relative humidity.

#### Theoretical calculations

All the calculations were carried out using the Vienna Ab initio Simulation Package (VASP) in the framework of the density functional theory (DFT), with the OPTPBE functional, which takes into account weak interactions (i.e., van der Waals forces). Periodic boundary conditions (PBC) were included in the calculation, allowing us a correct representation of the crystalline nature of the materials.

The electron density was expanded on a plane-wave basis, which is the ideal basis set to deal with periodic systems, such as those studied in this work. We included plane waves up to a cutoff energy of 450 eV, while the interactions between nuclei and electrons were described with the projector augmented wave (PAW) pseudopotentials, as provided in the VASP database. Reciprocal space was sampled with the  $\Gamma$ -point.

We used as the convergence criterium  $10^{-5}$  eV for the electron density. During the optimizations, we imposed all the Hellmann–Feynman forces to be lower than 0.01 eV/Å.

### 3. Results and Discussion

#### Structural Characterization

The reaction carried out in water under hydrothermal conditions (120 °C for 48 h) in a 1:4:2 stoichiometric ratio, (copper(II) nitrate trihydrate, 4,4-bipyridine (**bipy**), and 5-fluorouracil-1-acetic acid (**5-FUA**)) at pH around 2.3 produced several crystalline phases, some of them containing oxalate ( $(\text{C}_2\text{O}_4)^{2-} = \text{ox}$ ), acting as a bridging ligand. This experimental observation can be rationalized, taking into account previous reports in which the use of solvothermal conditions, in combination with acid pH values and the presence of copper(II) as a catalyst and reducing agent, produced an in situ decarboxylation of carboxyl groups. Thus, the carboxylic acid group became  $\text{CO}_2$ , which was promoted to  $(\text{C}_2\text{O}_4)^{2-}$  in the presence of  $\text{Cu}^{2+}$ , via a reduction reaction [43–45].

The careful observation at different times of the reaction mixture inside of the reactor (Table 1) and the mother liquor after filtration (Table 2), and the manual separation of the appearing single crystals allowed us to identify eight different crystalline phases, and to study the transformations between them. Interestingly, all the copper(II) compounds were pleochroic, showing important variations in their color depending on the orientation (Figure 1), which made more challenging the visual identification and separation of the phases.

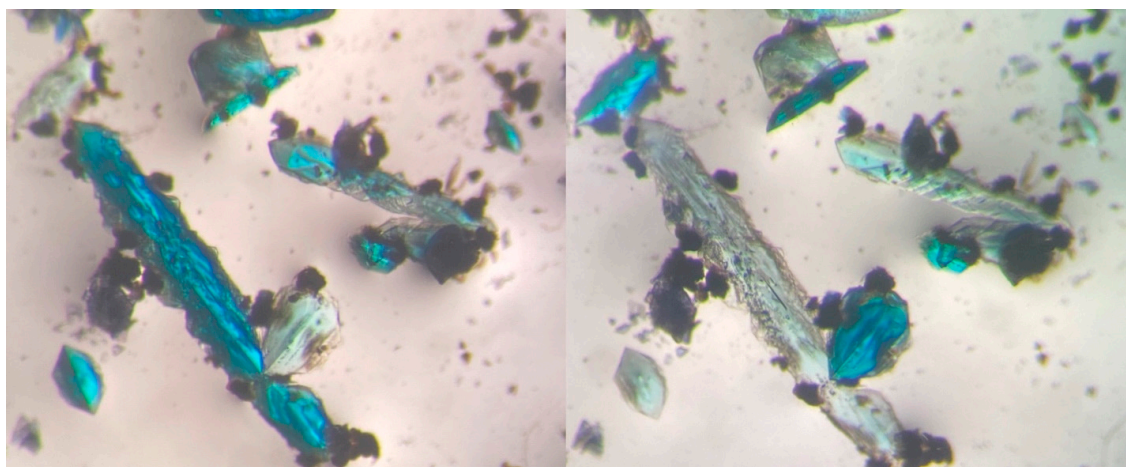


**Table 1.** Evolution of the coordination compounds (CCs) inside of the hydrothermal reactor from time 0 to 1 month.

Time	0 (Initial)	$\frac{1}{2}$ Day	6 Days	30 Days
CCs and concentration variation	$[(\text{H}_2\text{bipy})^{+2} 2\text{NO}_3^-] (1)$	Stable	Decrease	Decrease
	$[\text{Cu}_2(5\text{-FUA})_2(\text{ox})(\text{bipy})]_n \cdot 2n \text{H}_2\text{O} (\text{CP2})$	Stable	Decrease	$[\text{Cu}_3(\text{ox})_3(\text{bipy})_4]_n$ $[\text{Cu}(\text{ox})(\text{bipy})]_n$
	$[\text{Cu}(5\text{-FUA})_2(\text{H}_2\text{O})(\text{bipy})]_n \cdot 2n \text{H}_2\text{O} (\text{CP3})$	Increase	Increase	Decrease
		$[\text{Cu}(5\text{-FUA})_2(\text{bipy})]_n \cdot 3.5n \text{H}_2\text{O}$	Increase	Increase

**Table 2.** Evolution of the coordination compounds (CCs) in the mother liquor after filtration from time 0 to 6 days.

Time	$\frac{1}{2}$ Day	6 Days	30 Days
CCs and concentration variation		$[\text{Cu}(5\text{-FUA})_2(\text{H}_2\text{O})_4] \cdot 4\text{H}_2\text{O}$	Increase
	$[\text{Cu}(5\text{-FUA})_2(\text{H}_2\text{O})(\text{bipy})]_n \cdot 2n \text{H}_2\text{O} (\text{CP3})$	Increase	Decrease
	$[\text{Cu}(5\text{-FUA})_2(\text{bipy})]_n \cdot 3.5n \text{H}_2\text{O}$	Increase	Increase

**Figure 1.** Color change under polarized light of pleochroic crystals from compound  $[\text{Cu}_2(\text{ox})(\text{bipy})]_n$ .

As described in the synthesis section, as soon as the hydrothermal reaction finished, two types of blue crystals, together with aggregates of yellow solid, were observed inside the reactor (Figures 2a and S1). Some of the mother liquor was separated from the reaction mixture and left at room temperature.

In the isolated mixture, we observed that the yellow solid was composed of very small yellow crystals that partially dissolved if left in the mother liquor (Figure 2b,c). The IR spectrum of compound 1 showed bands at 3062 and 2938  $\text{cm}^{-1}$  corresponding to the  $\nu(\text{C-H})$  stretching vibrations, as well as bands around 1641 and 806  $\text{cm}^{-1}$  attributed to out-of-plane  $\nu(\text{C-H})$  stretching vibrations of the pyridine ring [46]. In addition, the vibrational peak for  $\text{N=O}$  stretching appeared at 1720  $\text{cm}^{-1}$ . The  $\text{NO}_3^-$  asymmetric and symmetric stretching vibrations appeared at 1347 and 867  $\text{cm}^{-1}$ , respectively, supporting the presence of  $\text{NO}_3^-$  as a counterion (Figure S4) [47]. Finally, single crystals of adequate size for SCXRD analysis were obtained (Figure S9 and Tables S1 and S2). It was found to be a new polymorph of the ionic solid with formula  $[(\text{H}_2\text{bipy})^{+2} 2\text{NO}_3^-]$  and did not contain any copper ions.

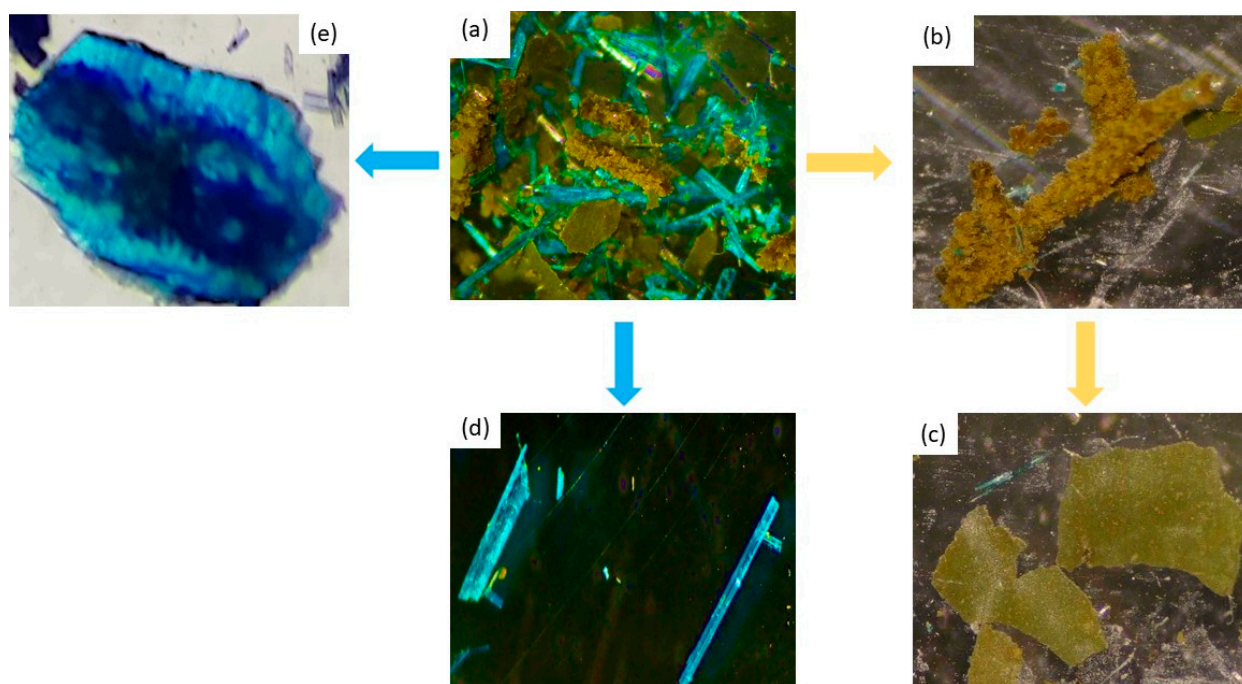


**Figure 2.** Initial mixture of yellow solid, together with pale-blue needle-shaped crystals (a). Poly-crystalline yellow samples of  $[(H_2bipy)^{+2} 2.NO_3^-]$  (1) (b,c). Pale blue needle-shaped crystals of  $[Cu_2(5-FUA)_2(ox)(bipy)]_n \cdot 2nH_2O$  (CP2), (d), and  $[Cu(5-FUA)_2(H_2O)(bipy)]_n \cdot 2nH_2O$  (CP3) (e).

One of the blue phases appeared as deep blue/turquoise crystals in the shape of long needles or ribbons, mostly forming aggregates (Figure 2d). The IR spectrum of this compound showed bands indicative of the presence of 5-FUA, oxalate, and bipyridine, displaced with respect to the starting ligands, indicating coordination to the metal center. The asymmetric and symmetric  $\nu COO^-$  appeared at  $1681$  and  $1401\text{ cm}^{-1}$ , respectively [48]. In addition, the bands corresponding to  $\nu_{as}$  and  $\nu_s$  of  $C=O$  could be assigned at  $1654$  and  $1401\text{ cm}^{-1}$ , respectively, indicative of oxalate acting as a bridging ligand. The vibrations corresponding to the  $\nu CH$  of the aromatic ring were at  $1592$  and  $1372\text{ cm}^{-1}$ . Single crystals were isolated from the reaction mixture and analyzed by SCXRD, resulting in a new 2D polymer with formula  $[Cu_2(5-FUA)_2(ox)(bipy)]_n \cdot 2nH_2O$  (CP2) (Figures 3 and S10, and Tables S3 and S4). The structure could be described as wavy layers parallel to the (110) plane where the metal atoms were joined by the three ligands (5-FUA, ox, and bipy) acting as ditopic connectors. The oxalate ligands linked copper atoms along the [110] direction in a  $\mu-1\kappa^2O, O':2\kappa^2O'', O'''$  mode, alternating with the 4,4'-bipy ligands (as ditopic  $\mu-1\kappa N:2\kappa N'$ ), that connected the metals in the same direction. Lastly, the carboxylate group in the 5-FUA ligands acted as a bridge in the [100] direction to complete the  $CuO_5N$  coordination environment. This resulted in an arrangement within the layers of pairs of  $Cu-O-Cu-O$  chains parallel to the [100] direction, where the copper atoms were located at a distance of  $4.734\text{ \AA}$ . There were numerous hydrogen bonds present, not only intralayer, but also between the sheets, involving the interstitial water molecules located between the 2D polymers (Figure 3). In addition, its elemental analysis matched the chemical formula obtained and its powder X-ray diffractogram showed the presence of a single crystalline phase coincident with the theoretical X-ray diffractogram obtained from single crystal X-ray diffraction (Figure S6).

If these crystals were left in the mother liquor, they began to show cracks after a few days, losing crystallinity and partially redissolving to yield  $[Cu(ox)(bipy)]_n$  and  $[Cu_3(ox)_3(bipy)_4]_n$  (Table 1 and Figure S2b,c).

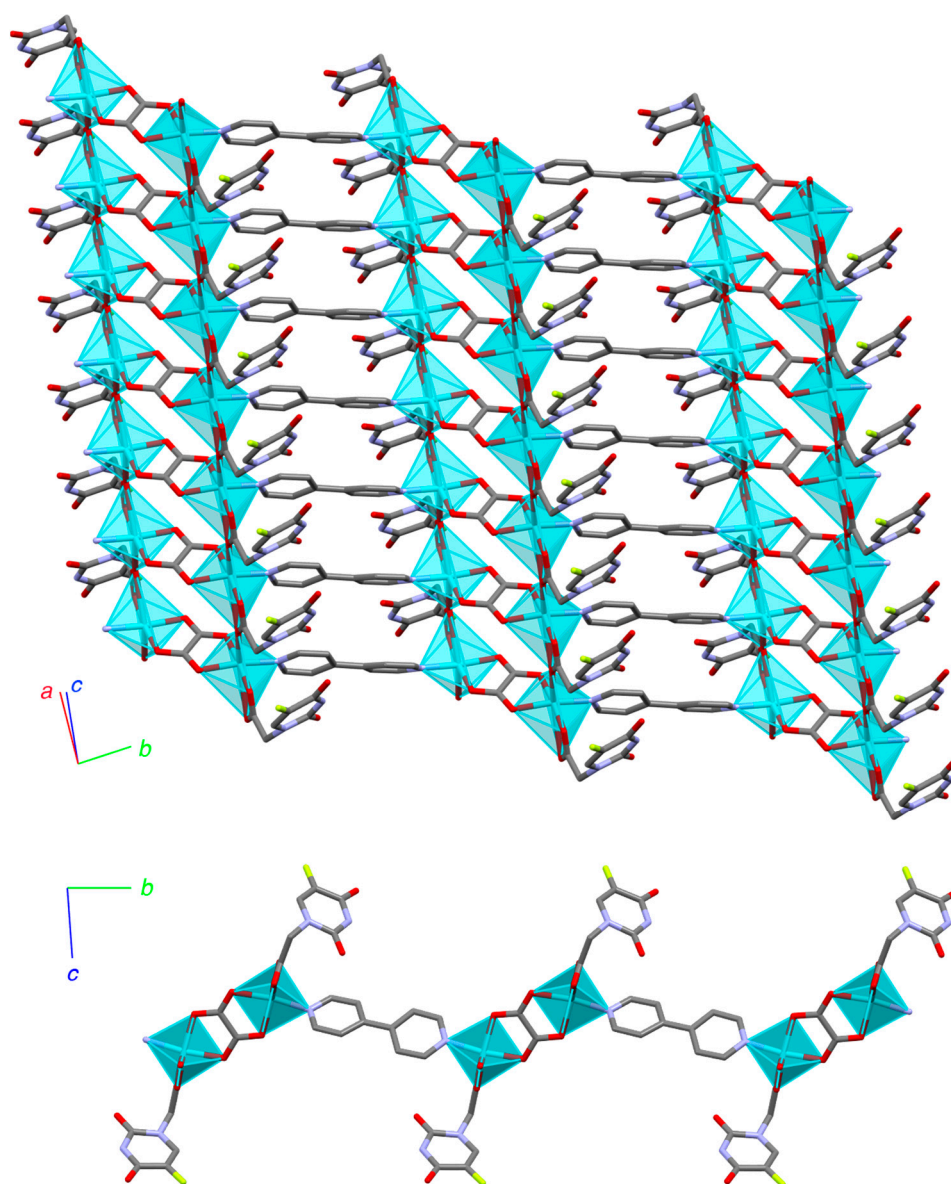


**Figure 3.** Layer of  $[\text{Cu}_2(5\text{-FUA})_2(\text{ox})(\text{bipy})]_n \cdot 2n\text{H}_2\text{O}$  (CP2): (top) zenithal view of the layer; (bottom) lateral view, both with crystallographic axes. Cyan polyhedra represent the copper coordination environments.

Another type of blue crystal, plate-shaped and dichroic (from intense blue to cyan), appeared as stacked aggregates (Figure 2e). This crystalline phase constituted a new 1D polymer that did not contain the oxalate ligand, with formula  $[\text{Cu}(5\text{-FUA})_2(\text{H}_2\text{O})(\text{bipy})]_n \cdot 2n\text{H}_2\text{O}$  (CP3, Figure 4, top). In this structure, only the bipyridine ligand acted as a connector along the growth direction of the polymer (parallel to  $[010]$ ) in a ditopic  $\mu\text{-}1\kappa\text{N}:2\kappa\text{N}'$  fashion, and all of 5-FUA ligands were terminal, half of them coordinating to a copper atom in a  $1\kappa^2\text{O}, \text{O}'$  chelating mode and the other half as monodentate  $1\kappa\text{O}$  (Figure S11 and Tables S5 and S6). There was also a coordinated water molecule per copper atom completing the distorted octahedral  $\text{CuO}_4\text{N}_2$  environment. As with  $[\text{Cu}_2(5\text{-FUA})_2(\text{ox})(\text{bipy})]_n \cdot 2n\text{H}_2\text{O}$  (CP2), there were numerous hydrogen bonds present between the polymers, involving the interstitial water molecules located between them (Table S11).



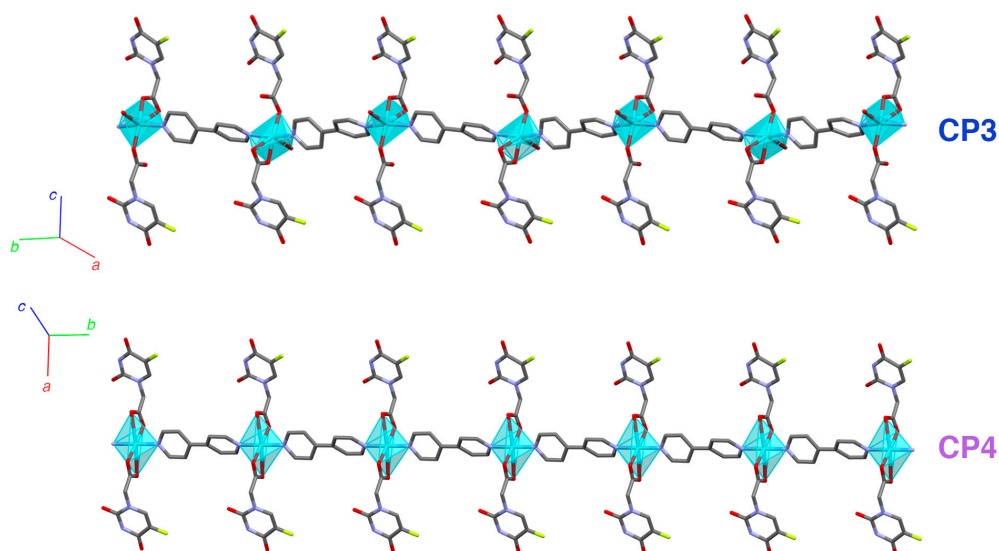


**Figure 4.** Coordination polymeric chains of compounds **CP3** (top) and **CP4** (bottom), both with crystallographic axes. Cyan polyhedra represent the copper coordination environments.

**CP3** was obtained with a low yield. The powder X-ray diffractogram of the sample allowed us to conclude that we had a single crystalline phase coincident with the theoretical X-ray diffractogram obtained from single-crystal X-ray diffraction (Figure S7).

A small violet plate appeared after a few hours, but only in the upper parts of the walls of the reactor that were not covered in the solution, representing a new monodimensional CP with formula  $[\text{Cu}(\text{5-FUA})_2(\text{bipy})]_n \cdot 2n\text{H}_2\text{O}$  (**CP4**, Figure 4, bottom) that could also be obtained when phase  $[\text{Cu}(\text{5-FUA})_2(\text{H}_2\text{O})(\text{bipy})]_n \cdot 2n\text{H}_2\text{O}$  (**CP3**) was exposed to the ambient atmosphere, constituting a reversible single-crystal to single-crystal transformation.

When exposed to humidity or submerged in the mother liquor, the violet crystals quickly reverted to blue  $[\text{Cu}(\text{5-FUA})_2(\text{H}_2\text{O})(\text{bipy})]_n \cdot 2n\text{H}_2\text{O}$  (**CP3**) (Figure 5). To confirm that the crystallinity of the solid was preserved, and to prove the SCSC nature of the conversion, the same single crystal previously used for the structure solution of **CP3** was left in ambient conditions until the color change was complete. After 2 days, it was submitted to a new SCXRD experiment, and the structure of **CP4** was solved from that data collection (Figure S12 and Tables S7 and S8).

The main difference between these two 1D polymers was the absence of the coordinated water molecule present in the blue crystals, and the subsequent approximation of the previously non-coordinated carboxylic oxygen atom from half of the 5-FUA ligands. To achieve this transformation, the coordinated water molecule was lost (Cu–O distance 2.341 Å), and the previously non-coordinated carboxylic oxygen atom from half of the 5-FUA ligands approximated to the nearest metal center in order to complete the  $\text{CuN}_2\text{O}_4$  coordination environment, changing its distance to the metal from 3.152 to 2.608 Å. This small rearrangement did not substantially modify the overall crystal structure, allowing the reversibility of the SCSC transformation. The fact that the coordinated water molecule was lost (causing the change in color) and the interstitial molecules remained was previously observed in our research [49]. This could be explained by the fact that these interstitial water molecules were involved in numerous hydrogen bonds (see Table S11), and the energy needed to remove them was larger than that required to extract the molecule that is within the coordination sphere.

This transformation, accompanied by an important change in color, allowed us to postulate the possible use of this compound as a sensor of environmental humidity. To determine the degree of sensitivity, compound  $[\text{Cu}(\text{5-FUA})_2(\text{bipy})]_n \cdot 2n\text{H}_2\text{O}$  (**CP4**) (violet) was placed in a dry box with relative humidity control (Figure 6). The experiment showed that, at humidity levels around 70%, the transformation to the compound  $[\text{Cu}(\text{5-FUA})_2(\text{H}_2\text{O})(\text{bipy})]_n \cdot 2n\text{H}_2\text{O}$  (**CP3**) (blue) was observed.



$\text{FUA}_2(\text{H}_2\text{O})(\text{bipy})_n \cdot 2n\text{H}_2\text{O}$  (CP3) (blue) occurred. The process was reversible and reproducible. Indeed, the experiment was repeated up to three times to check the reversibility at different temperatures (20, 30, and 40 °C). CP3 took 25 to 30 min to fully convert to CP4 always at the same humidity percentage. In addition, the CP4 elemental analysis obtained after the transformation matched with the chemical formula, and its X-ray powder diffractogram confirmed the obtention of a single crystalline phase coinciding with the theoretical X-ray diffractogram obtained by single-crystal X-ray diffraction (Figure S8).

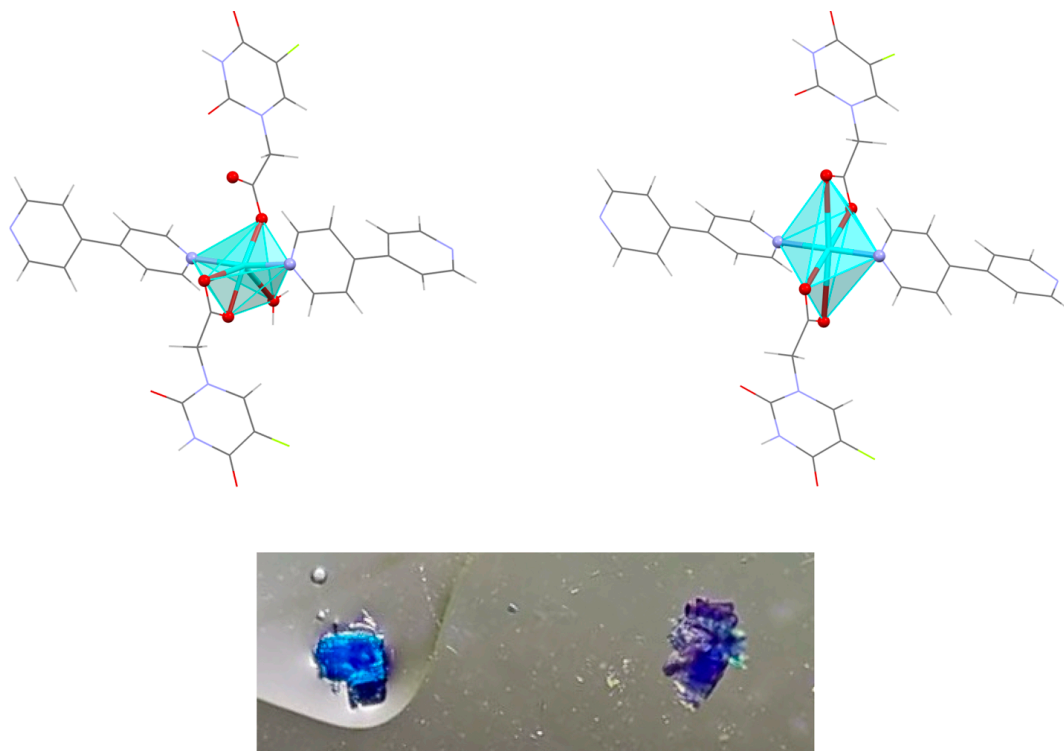


**Figure 5.** Reversible single-crystal to single-crystal transformation of CP3 (left, in a drop of water) into CP4 (right, exposed to air). Cyan polyhedra represent the copper coordination environments.

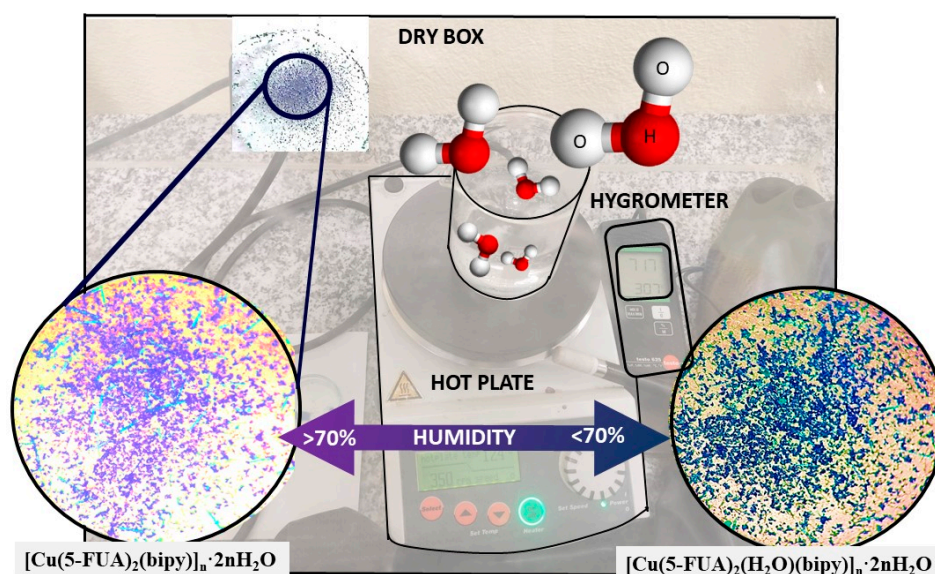


**Figure 6.** Diagram of the experiment carried out to measure the degree of humidity and the color change of  $[\text{Cu}(5\text{-FUA})_2(\text{bipy})]_n \cdot 2n\text{H}_2\text{O}$  (CP4) (violet) and  $[\text{Cu}(5\text{-FUA})_2(\text{H}_2\text{O})(\text{bipy})]_n \cdot 2n\text{H}_2\text{O}$  (CP3) (blue) compounds.

Bearing in mind the importance of humidity in the conservation of buildings, in the comfort of homes, where the current regulations for thermal installations establish that the relative humidity inside buildings must be around 45–75% both compounds could serve as low-cost, real-time, in situ visualization and easy-to-handle humidity colorimetric sensors [36,50–53].

DFT calculations allowed us to understand the reversibility of this process. Using a large unit cell ( $n = 8$ , optimized structures are shown in Figure S14),  $[\text{Cu}(\text{5-FUA})_2(\text{H}_2\text{O})(\text{bipy})]_n \cdot 2n\text{H}_2\text{O}$  was found to be 4.86 eV more stable than  $[\text{Cu}(\text{5-FUA})_2(\text{bipy})]_n \cdot 2n\text{H}_2\text{O} + 8$  isolated water molecules (see Table 3). However, if these molecules presented intermolecular interactions (e.g., in liquid phase), the relative stability reverted, and  $[\text{Cu}(\text{5-FUA})_2(\text{bipy})]_n \cdot 2n\text{H}_2\text{O}$  became 0.11 eV more stable. Therefore, the observed crystalline phases were determined not only by their intrinsic properties, but also by the medium, since external conditions could shift the equilibrium.

**Table 3.** Relative energy of the two phases with potential application as humidity sensor.

Compound	Relative Energy (eV)
$[\text{Cu}(\text{5-FUA})_2(\text{H}_2\text{O})(\text{bipy})]_n \cdot 2n\text{H}_2\text{O}$	0.00
$[\text{Cu}(\text{5-FUA})_2(\text{bipy})]_n \cdot 2n\text{H}_2\text{O} + 8\text{H}_2\text{O}$ (isolated)	4.86
$[\text{Cu}(\text{5-FUA})_2(\text{bipy})]_n \cdot 2n\text{H}_2\text{O} + 8\text{H}_2\text{O}$ (condensed phase)	−0.11

After several days, two different crystal phases appeared inside of the reactor: small pale blue needles of  $[\text{Cu}_3(\text{ox})_3(\text{bipy})_4]_n$  and blue crystals of  $[\text{Cu}(\text{ox})(\text{bipy})]_n$  (Figure S2).

The blue needles (pale blue/turquoise) were isolated and identified as the 2D coordination polymer  $[\text{Cu}_3(\text{ox})_3(\text{bipy})_4]_n$ , previously reported by Castillo et al. [54] and deposited in the CSD with code IJASAN. This phase could only be found at the early stages, spontaneously dissolving in the mother liquor unless filtered and separated from the mixture. The polymer consisted of copper(II) centers coordinated by oxalato ligands acting as  $\mu\text{-}1\kappa^2\text{O},\text{O}':2\kappa^2\text{O}'',\text{O}'''$  bridges in the [010] direction to form chains. These chains were linked by ditopic  $\mu\text{-}1\kappa\text{N}:2\kappa\text{N}'$  4,4'-bipy ligands, alternating with terminal bipy moieties, resulting in two-dimensional layers parallel to the (102) plane. Each metal atom was connected to three adjacent copper atoms (two in the same row and another from a neighboring one), presenting a distorted octahedral  $\text{CuO}_4\text{N}_2$  coordination environment.

Another bidimensional coordination polymer appeared as dichroic pale green/intense blue crystals, in the shape of elongated prisms with a rhombic section. This phase started as very small needles that underwent an Ostwald ripening process and coalesced to yield larger crystals. They were identified as the compound  $[\text{Cu}(\text{ox})(\text{bipy})]_n$ , also reported in the literature [55] and deposited in the CSD with code UDOGEA01. The crystal structure of this polymer consisted of layers, in this case parallel to the (011) plane, containing copper(II) centers in distorted octahedral  $\text{CuO}_4\text{N}_2$  coordination environments. The oxalate ligands also acted as  $\mu\text{-}1\kappa^2\text{O},\text{O}':2\kappa^2\text{O}'',\text{O}'''$  bridges, here in the [001] direction, to yield rows linked in the [010] direction by the 4,4'-bipy ligands; in this case, all of them were ditopic  $\mu\text{-}1\kappa\text{N}:2\kappa\text{N}'$ . Each metal atom was connected to four adjacent copper atoms (two in the same row and two from the neighboring ones).

On the other hand, if the mother liquor was separated from the reaction mixture, only the monodimensional polymers  $[\text{Cu}(\text{5-FUA})_2(\text{H}_2\text{O})(\text{bipy})]_n \cdot 2n\text{H}_2\text{O}$  (CP3) (as well as the dehydrated  $[\text{Cu}(\text{5-FUA})_2(\text{bipy})]_n \cdot 2n\text{H}_2\text{O}$  (CP4) when the walls of the recipient were no longer covered in the solution) and  $[\text{Cu}(\text{5-FUA})_2(\text{bipy})]_n \cdot 3.5n\text{H}_2\text{O}$  were found, together with  $[\text{Cu}(\text{5-FUA})_2(\text{H}_2\text{O})_4] \cdot 4\text{H}_2\text{O}$  (Figure 7 and Figure S3).

The structure of the purple plate-shaped crystals of polymeric  $[\text{Cu}(\text{5-FUA})_2(\text{bipy})]_n \cdot 3.5n\text{H}_2\text{O}$  was recently reported by our group [31] and deposited in the CSD with code ECAQEI. It is a ladder-type 1D coordination polymer with formula  $[\text{Cu}(\text{5-FUA})_2(\text{bipy})]_n \cdot 3.5n\text{H}_2\text{O}$ , where the bipyridine acts as a  $\mu\text{-}1\kappa\text{N}:2\kappa\text{N}'$  connector. Half of the 5-FUA ligands

act as bridges in a  $\mu$ -1:2 $\kappa$ O fashion (Cu...Cu distance is 3.396 Å), and the other half are monodentate 1 $\kappa$ O.

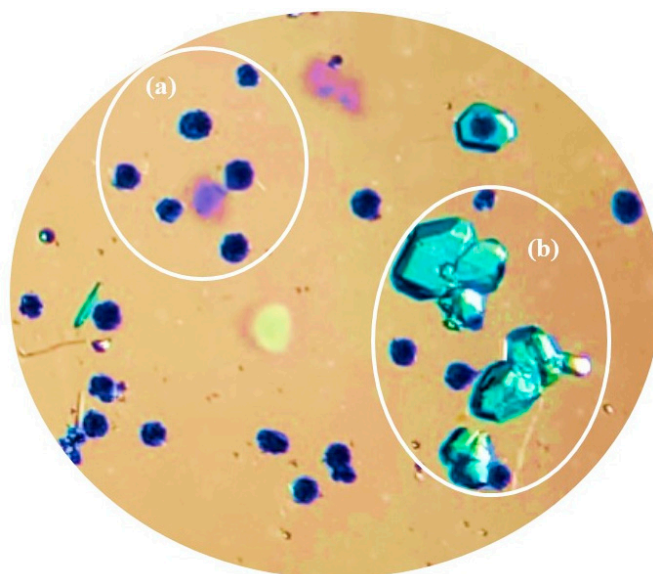


**Figure 7.** Optical image of  $[\text{Cu}(\text{5-FUA})_2(\text{bipy})]_n \cdot 3.5n\text{H}_2\text{O}$  (a) and  $[\text{Cu}(\text{5-FUA})_2(\text{H}_2\text{O})_4] \cdot 4\text{H}_2\text{O}$  (b) in the separated mother liquor.

The last crystalline phase identified appeared as large dichroic (turquoise/deep blue) prisms and was found to be a molecular coordination compound with formula  $[\text{Cu}(\text{5-FUA})_2(\text{H}_2\text{O})_4] \cdot 4\text{H}_2\text{O}$  (Figure S13d), previously reported [56] and deposited in the CSD with code XAXMEO. In this compound, the copper atom adopted a  $\text{CuO}_6$  octahedral environment where the four equatorial positions were occupied by water molecules and the two axial ones were occupied by carboxylic oxygen atoms from terminal 5-FUA ligands (1 $\kappa$ O).

#### 4. Conclusions

The present study unveiled the remarkable uniqueness of coordination compounds, highlighting their structural versatility. The variations in synthetic conditions and the dynamic nature of coordination bonds confirmed the boundless architectural possibilities and diverse properties inherent in these materials. Moreover, by employing more aggressive synthesis methods, we successfully obtained novel coordination environments and in situ transformations of the building blocks, often facilitated by the catalytic influence of the metal cation center. The low energy barriers between different environments facilitated the evolutionary behavior of these species over time.

This research expands the scope of structural possibilities explored thus far, employing Cu(II), 5-fluoro uracil-1-acetate, and 4,4-bipyridine. Specifically, the synthesis of the  $[\text{Cu}(\text{5-FUA})_2(\text{H}_2\text{O})(\text{bipy})]_n \cdot 2n\text{H}_2\text{O}$  compound in its solid state, along with its subsequent transformation to  $[\text{Cu}(\text{5-FUA})_2(\text{bipy})]_n \cdot 2n\text{H}_2\text{O}$  through a single-crystal to single-crystal (SCSC) process, demonstrates a pronounced color change. This phenomenon holds implications for potential applications, such as humidity sensing. Theoretical investigations have indicated that, although the compound with the coordinated water molecule exhibits greater energetic stability, the loss of the water molecule coordinated to the metallic center is favored by the formation of intermolecular bonds between them. Notably, an equilibrium between the two species was observed in the presence of approximately 70% humidity.

In summary, the research surpasses the existing state of the art by revealing novel synthetic pathways and transformations, leading to diverse architectural possibilities. The findings, particularly the SCSC transformation and the associated color change, hold useful for applications such as humidity sensing. Theoretical insights further illuminate

the delicate balance between stability and intermolecular interactions, highlighting the complex nature of these compounds.

**Supplementary Materials:** The following files are available free of charge: crystal transformations, chemical characterization of the compounds, and crystal structure data of the compounds (PDF, Checkcif, and CIF files; see DOI:10.1039/x0xx00000x). The following supporting information can be downloaded at <https://www.mdpi.com/article/10.3390/polym15132827/s1>: Figure S1. Microscope image ( $\times 2.0$  zoom) of phases detected in the reactor at initial time in the hydrothermal reaction corresponding with dark-blue crystal  $[\text{Cu}(\text{5-FUA})_2(\text{H}_2\text{O})(\text{bipy})]_n \cdot 2n\text{H}_2\text{O}$  (CP3) (a), elongated turquoise crystals  $[\text{Cu}_2(\text{5-FUA})_2(\text{ox})(\text{bipy})]_n \cdot 2n\text{H}_2\text{O}$  (CP2) (b), and yellow crystal of  $[(\text{H}_2\text{bipy})^{+2} 2.\text{NO}_3^{-}]$  (1) (c); Figure S2. Crystal of  $[\text{Cu}_2(\text{5-FUA})_2(\text{ox})(\text{bipy})]_n \cdot 2n\text{H}_2\text{O}$  (a) transformation to  $[\text{Cu}(\text{ox})(\text{bipy})]_n$  (b) and  $[\text{Cu}_3(\text{ox})_3(\text{bipy})_4]_n$  (c); Figure S3. Microscope image ( $\times 4.0$  zoom) of phases in the separated mother liquor:  $[\text{Cu}(\text{5-FUA})_2(\text{H}_2\text{O})(\text{bipy})]_n \cdot 2n\text{H}_2\text{O}$  (CP3) (a) and  $[\text{Cu}(\text{5-FUA})_2(\text{bipy})]_n \cdot 3.5n\text{H}_2\text{O}$  (b); Figure S4. IR spectrum of  $[(\text{H}_2\text{bipy})^{+2} 2.\text{NO}_3^{-}]$  (1); Figure S5. IR spectrum of  $[\text{Cu}_2(\text{5-FUA})_2(\text{ox})(\text{bipy})]_n \cdot 2n\text{H}_2\text{O}$  (CP2); Figure S6. X-ray diffractogram of  $[\text{Cu}_2(\text{5-FUA})_2(\text{ox})(\text{bipy})]_n \cdot 2n\text{H}_2\text{O}$  (CP2): theoretical (black line) and experimental (red line); Figure S7. X-ray diffractogram of  $[\text{Cu}(\text{5-FUA})_2(\text{H}_2\text{O})(\text{bipy})]_n \cdot 2n\text{H}_2\text{O}$  (CP3): theoretical (black line) and experimental (green line); Figure S8. X-ray diffractogram of  $[\text{Cu}(\text{5-FUA})_2(\text{bipy})]_n \cdot 2n\text{H}_2\text{O}$  (CP4): theoretical (black line) and experimental (blue line); Figure S9. Asymmetric unit of compound 1 with non-hydrogen atoms labeled; Table S1. Sample and crystal data for  $[(\text{H}_2\text{bipy})^{+2} 2.\text{NO}_3^{-}]$ ; Table S2. Data collection and structure refinement for 1; Figure S10. Asymmetric unit of compound  $[\text{Cu}_2(\text{5-FUA})_2(\text{ox})(\text{bipy})]_n \cdot 2n\text{H}_2\text{O}$  (CP2) with atoms labeled. Hydrogen atoms are omitted for clarity; Table S3. Sample and crystal data for CP2; Table S4. Data collection and structure refinement for CP2; Figure S11. Asymmetric unit of compound  $[\text{Cu}(\text{5-FUA})_2(\text{H}_2\text{O})(\text{bipy})]_n \cdot 2n\text{H}_2\text{O}$  (CP3) with atoms labeled. Hydrogen atoms are omitted for clarity; Table S5. Sample and crystal data for CP3; Table S6. Data collection and structure refinement for CP3; Figure S12. Asymmetric unit of compound  $[\text{Cu}(\text{5-FUA})_2(\text{bipy})]_n \cdot 2n\text{H}_2\text{O}$  (CP4) with atoms labeled. Hydrogen atoms are omitted for clarity; Table S7. Sample and crystal data for CP4; Table S8. Data collection and structure refinement for CP4; Figure S13. Coordination environments of copper atoms in the compounds with the resulting colors: (a) pair of  $\text{CuO}_4\text{N}_2$  octahedra from a zigzag row in  $[\text{Cu}_3(\text{ox})_3(\text{bipy})_4]_n$ ; (b) pair of  $\text{CuO}_4\text{N}_2$  octahedra from a linear row in  $[\text{Cu}(\text{ox})(\text{bipy})]_n$ ; (c) group of four  $\text{CuO}_5\text{N}$  polyhedra from a layer in  $[\text{Cu}_2(\text{5-FUA})_2(\text{ox})(\text{bipy})]_n \cdot 2n\text{H}_2\text{O}$  (CP2); (d)  $\text{CuO}_6$  octahedron in  $[\text{Cu}(\text{5-FUA})_2(\text{H}_2\text{O})_4] \cdot \text{H}_2\text{O}$ ; (e)  $\text{CuO}_4\text{N}_2$  polyhedron in  $[\text{Cu}(\text{5-FUA})_2(\text{H}_2\text{O})(\text{bipy})]_n \cdot 2n\text{H}_2\text{O}$  (CP3); (f) pair of edge-sharing square pyramids  $\text{CuO}_3\text{N}_2$  in  $[\text{Cu}(\text{5-FUA})_2(\text{bipy})]_n \cdot 2.25n\text{H}_2\text{O}$ ; (g) highly distorted  $\text{CuO}_4\text{N}_2$  octahedron in  $[\text{Cu}(\text{5-FUA})_2(\text{bipy})]_n \cdot 2n\text{H}_2\text{O}$  (CP4); Table S9. Selected coordination copper bond distances ( $\text{\AA}$ ) for compounds CP2, CP3, and CP4; Table S10. Selected copper coordination bond angles ( $^\circ$ ) for compounds CP2, CP3, and CP4; Table S11. Relevant supramolecular hydrogen bond interactions found in compounds CP2, CP3, and CP4. Interactions involving interstitial water molecules in blue, with the strongest ones in bold; Figure S14. Optimized structures of compounds  $[\text{Cu}(\text{5-FUA})_2(\text{H}_2\text{O})(\text{bipy})]_n \cdot 2n\text{H}_2\text{O}$  (CP3, top) and  $[\text{Cu}(\text{5-FUA})_2(\text{bipy})]_n \cdot 2n\text{H}_2\text{O}$  (CP4, bottom).

**Author Contributions:** Investigation, V.G.V.; investigation and formal analysis, A.G.-H.; formal analysis and writing—reviewing, F.A.-G.; investigation and writing—reviewing and editing, J.P.; conceptualization, investigation, methodology, supervision, resources, funding acquisition, project administration, and writing—original draft, review, and editing, P.A.-O. All authors have read and agreed to the published version of the manuscript.

**Funding:** This work was supported by the Spanish Ministerio de Ciencia e Innovación and Agencia Estatal de Investigación (MCIN/AEI/10.13039/501100011033; PID2019-108028GB-C22 and TED2021-131132B-C22). Calculations were performed thanks to the generous allocation of computing resources at Centro de Computación Científica (CCC-UAM). This work is dedicated to Lydia and Paula.

**Institutional Review Board Statement:** Not applicable.

**Data Availability Statement:** The data presented in this study are available on request from the corresponding author. The data are not publicly available due to privacy.

**Conflicts of Interest:** The authors declare no conflict of interest.



## References

- Batten, S.R.N.; Neville, S.M.; Turner, D. *Coordination Polymers: Design, Analysis and Applications*; RSC Publishing: Cambridge, UK, 2009; p. 7.
- Batten, S.R.; Chen, B.; Vittal, J.J. Coordination Polymers/MOFs: Structures, Properties and Applications. *Chempluschem* **2016**, *81*, 669–670. [[CrossRef](#)] [[PubMed](#)]
- Krasnovskaya, O.; Naumov, A.; Guk, D.; Gorelkin, P.; Erofeev, A.; Beloglazkina, E.; Majouga, A. Copper Coordination Compounds as Biologically Active Agents. *Int. J. Mol. Sci.* **2020**, *21*, 3965. [[CrossRef](#)] [[PubMed](#)]
- Hussain, A.; AlAjmi, M.F.; Rehman, M.T.; Amir, S.; Husain, F.M.; Alsalmeh, A.; Siddiqui, M.A.; AlKhedhairi, A.A.; Khan, R.A. Copper(II) complexes as potential anticancer and Nonsteroidal anti-inflammatory agents: In vitro and in vivo studies. *Sci. Rep.* **2019**, *9*, 5237–5254. [[CrossRef](#)] [[PubMed](#)]
- Jiang, H.-Y.; Zhou, P.; Wang, Y.; Duan, R.; Chen, C.; Song, W.; Zhao, J. Copper-Based Coordination Polymer Nanostructure for Visible Light Photocatalysis. *Adv. Mater.* **2016**, *28*, 9657–9868. [[CrossRef](#)] [[PubMed](#)]
- Troyano, J.; Perles, J.; Amo-Ochoa, P.; Martínez, J.I.; Zamora, F.; Delgado, S. Reversible recrystallization process of copper and silver thioacetamide-halide coordination polymers and their basic building blocks. *Crystengcomm* **2014**, *16*, 8224–8231. [[CrossRef](#)]
- Vegas, V.G.; Villar-Alonso, M.; Gómez-García, C.J.; Zamora, F.; Amo-Ochoa, P. Direct Formation of Sub-Micron and Nanoparticles of a Bioinspired Coordination Polymer Based on Copper with Adenine. *Polymers* **2017**, *9*, 565. [[CrossRef](#)]
- Amo-Ochoa, P.; Castillo, O.; Gómez-García, C.J.; Hassanein, K.; Verma, S.; Kumar, J.; Zamora, F. Semiconductive and Magnetic One-Dimensional Coordination Polymers of Cu(II) with Modified Nucleobases. *Inorg. Chem.* **2013**, *52*, 11428–11437. [[CrossRef](#)]
- Usman, M.; Mendiratta, S.; Lu, K.-L. Semiconductor Metal-Organic Frameworks: Future Low-Bandgap Materials. *Adv. Mater.* **2017**, *29*, 1605071. [[CrossRef](#)] [[PubMed](#)]
- Dennehy, M.; Amo-Ochoa, P.; Freire, E.; Suárez, S.; Halac, E.; Baggio, R. Structure and electrical properties of a one-dimensional polymeric silver thiosaccharinate complex with argentophilic interactions. *Acta Crystallogr.* **2018**, *74*, 186–193. [[CrossRef](#)]
- Amo-Ochoa, P.; Alexandre, S.S.; Hribesh, S.; Galindo, M.A.; Castillo, O.; Gómez-García, C.J.; Pike, A.R.; Soler, J.M.; Houlton, A.; Harrington, R.W. Coordination Chemistry of 6-Thioguanine Derivatives with Cobalt: Toward Formation of Electrical Conductive One-Dimensional Coordination Polymers. *Inorg. Chem.* **2013**, *52*, 7306. [[CrossRef](#)]
- Rowsell, J.L.C.; Yaghi, O.M. Metal-organic frameworks: A new class of porous materials. *Microporous Mesoporous Mater.* **2004**, *73*, 3–14. [[CrossRef](#)]
- Furukawa, H.; Cordova, K.E.; O’Keeffe, M.; Yaghi, O.M. The Chemistry and Applications of Metal-Organic Frameworks. *Science* **2013**, *341*, 974–989. [[CrossRef](#)] [[PubMed](#)]
- Wang, X.; McHale, R. Metal-Containing Polymers: Building Blocks for Functional (Nano)Materials. *Macromol. Rapid Commun.* **2010**, *31*, 331–350. [[CrossRef](#)] [[PubMed](#)]
- Chen, Y.; Wang, Z.-O.; Ren, Z.-G.; Li, H.-X.; Li, D.-X.; Liu, D.; Zhang, Y.; Lang, J.-P. Solvothermal Stepwise Formation of Cu/I/S-Based Semiconductors from a Three-Dimensional Net to One-Dimensional Chains. *Cryst. Growth Des.* **2009**, *9*, 4963–4968. [[CrossRef](#)]
- Chen, X.-M.; Tong, M.-L. Solvothermal in Situ Metal/Ligand Reactions: A New Bridge between Coordination Chemistry and Organic Synthetic Chemistry. *Acc. Chem. Res.* **2007**, *40*, 162–170. [[CrossRef](#)]
- Han, Z.-P.; Li, Y. Solvothermal synthesis, structure and catalytic activity of a mixed-valence CuI/CuII complex with 1-D chain structure. *Inorg. Chem. Commun.* **2012**, *22*, 73–76. [[CrossRef](#)]
- Murillo, M.; García-Hernán, A.; López, J.; Perles, J.; Brito, I.; Amo-Ochoa, P. The flexibility of CuI chains and the functionality of pyrazine-2-thiocarboxamide keys to obtaining new Cu(I)-I coordination polymers with potential use as photocatalysts for organic dye degradation. *Catal. Today* **2023**, *418*, 114072–114081. [[CrossRef](#)]
- Cheng, L.; Zhang, W.-X.; Ye, B.-H.; Lin, J.-B.; Chen, X.-M. In Situ Solvothermal Generation of 1,2,4-Triazolates and Related Compounds from Organonitrile and Hydrazine Hydrate: A Mechanism Study. *Inorg. Chem.* **2007**, *46*, 1135–1143. [[CrossRef](#)]
- Das, M.C.; Bharadwaj, P.K. A Porous Coordination Polymer Exhibiting Reversible Single-Crystal to Single-Crystal Substitution Reactions at Mn(II) Centers by Nitrile Guest Molecules. *J. Am. Chem. Soc.* **2009**, *131*, 10942–10949. [[CrossRef](#)]
- Kobayashi, A.; Kato, M. Stimuli-responsive Luminescent Copper(I) Complexes for Intelligent Emissive Devices. *Chem. Lett.* **2017**, *46*, 154–162. [[CrossRef](#)]
- Chen, W.-H.; Liao, W.-C.; Sohn, Y.S.; Fadeev, M.; Ceconello, A.; Nechushtai, R.; Willner, I. Stimuli-Responsive Nucleic Acid-Based Polyacrylamide Hydrogel-Coated Metal-Organic Framework Nanoparticles for Controlled Drug Release. *Adv. Funct. Mater.* **2018**, *28*, 1705137–1705146. [[CrossRef](#)]
- Nishikawa, M.; Kume, S.; Nishihara, H. Stimuli-responsive pyrimidine ring rotation in copper complexes for switching their physical properties. *Phys. Chem. Chem. Phys.* **2013**, *15*, 10549–10565. [[CrossRef](#)] [[PubMed](#)]
- Burneo, I.; Stylianou, K.C.; Rodríguez-Hermida, S.; Juanhuix, J.; Fontrodona, X.; Imaz, I.; MasPOCH, D. Two New Adenine-Based Co(II) Coordination Polymers: Synthesis, Crystal Structure, Coordination Modes, and Reversible Hydrochromic Behavior. *Cryst. Growth Des.* **2015**, *15*, 3182–3189. [[CrossRef](#)]
- Ke, S.-Y.; Chang, Y.-F.; Wang, H.-Y.; Yang, C.-C.; Ni, C.-W.; Lin, G.-Y.; Chen, T.-T.; Ho, M.-L.; Lee, G.-H.; Chuang, Y.-C.; et al. Self-Assembly of Four Coordination Polymers in Three-Dimensional Entangled Architecture Showing Reversible Dynamic Solid-State Structural Transformation and Color-Changing Behavior upon Thermal Dehydration and Rehydration. *Cryst. Growth Des.* **2014**, *14*, 4011–4018. [[CrossRef](#)]

26. Li, Y.; Zhao, B.; Xue, J.-P.; Xie, J.; Yao, Z.-S.; Tao, J. Giant single-crystal-to-single-crystal transformations associated with chiral interconversion induced by elimination of chelating ligands. *Nat. Commun.* **2021**, *12*, 6908–6917. [[CrossRef](#)] [[PubMed](#)]
27. Mahmoudi, G.; Morsali, A. Crystal-to-Crystal Transformation from a Weak Hydrogen-Bonded Two-Dimensional Network Structure to a Two-Dimensional Coordination Polymer on Heating. *Cryst. Growth Des.* **2008**, *8*, 391–394. [[CrossRef](#)]
28. Sarma, D.; Natarajan, S. Usefulness of in Situ Single Crystal to Single Crystal Transformation (SCSC) Studies in Understanding the Temperature-Dependent Dimensionality Cross-over and Structural Reorganization in Copper-Containing Metal–Organic Frameworks (MOFs). *Cryst. Growth Des.* **2011**, *11*, 5415–5423. [[CrossRef](#)]
29. Arriñez-Soriano, J.; Albalad, J.; Vila-Parrondo, C.; Pérez-Carvajal, J.; Rodríguez-Hermida, S.; Cabeza, A.; Juanhuix, J.; Imaz, I.; MasPOCH, D. Single-crystal and humidity-controlled powder diffraction study of the breathing effect in a metal–organic framework upon water adsorption/desorption. *Chem. Commun.* **2016**, *52*, 7229–7232. [[CrossRef](#)]
30. Daszkiewicz, M.; Puszyńska-Tuszkano, M.; Staszak, Z.; Chojnacka, I.; Fałtynowicz, H.; Cieślak-Golonka, M. Single crystal-to-single crystal transformations induced by ammonia–water equilibrium changes. *Crystengcomm* **2018**, *20*, 2907–2911. [[CrossRef](#)]
31. Vegas, V.G.; Latorre, A.; Marcos, M.L.; Gómez-García, C.J.; Castillo, O.; Zamora, F.; Gómez, J.; Martínez-Costas, J.; López, M.V.; Somoza, A.; et al. Rational Design of Copper(II)–Uracil Nanoprocessed Coordination Polymers to Improve Their Cytotoxic Activity in Biological Media. *ACS Appl. Mater. Interfaces* **2021**, *13*, 36948–36957. [[CrossRef](#)]
32. Rao, X.; Zhao, L.; Xu, L.; Wang, Y.; Liu, K.; Wang, Y.; Chen, G.Y.; Liu, T.; Wang, Y. Review of Optical Humidity Sensors. *Sensors* **2021**, *21*, 8049. [[CrossRef](#)] [[PubMed](#)]
33. Montes-García, V.; Samori, P. Humidity Sensing with Supramolecular Nanostructures. *Adv. Mater.* **2022**, 2208766. [[CrossRef](#)]
34. Chou, K.-S.; Lee, T.-K.; Liu, F.-J. Sensing mechanism of a porous ceramic as humidity sensor. *Sens. Actuators B Chem.* **1999**, *56*, 106–111. [[CrossRef](#)]
35. Li, Y.; Yang, M.; Camaioni, N.; Casalbore-Miceli, G. Humidity sensors based on polymer solid electrolytes: Investigation on the capacitive and resistive devices construction. *Sens. Actuators B Chem.* **2001**, *77*, 625–631. [[CrossRef](#)]
36. Coleman, J.R.; Meggers, F. Sensing of Indoor Air Quality—Characterization of Spatial and Temporal Pollutant Evolution Through Distributed Sensing. *Front. Built Environ.* **2018**, *4*, 28. [[CrossRef](#)]
37. McMullan, R. *Environmental Science in Building*; Bloomsbury Publishing: London, UK, 2017.
38. Masao, T. Antineoplastic Agents. The Preparation of 5-Fluorouracil-1-acetic Acid Derivatives. *Bull. Chem. Soc. Jpn.* **1975**, *48*, 3427–3428. [[CrossRef](#)]
39. Sheldrick, G.M. *SADABS, Program for Area Detector Adsorption Correction*; Institute for Inorganic Chemistry, University of Gottingen: Göttingen, Germany, 1996.
40. Bruker; AXS Inc.: Madison, WI, USA, 2012.
41. Sheldrick, G.M. SHELXT-Integrated Space-Group and Crystal-Structure Determination. *Acta Cryst.* **2015**, *71*, 3–8. [[CrossRef](#)] [[PubMed](#)]
42. Sheldrick, G.M. *SHELXL-97, Program for Crystal Structure Refinement*; University Gottingen: Gottingen, Germany, 1997.
43. Frisch, M.; Cahill, C.L. In situ ligand synthesis with the UO<sub>2</sub><sup>2+</sup> cation under hydrothermal conditions. *J. Solid State Chem.* **2007**, *180*, 2597–2602. [[CrossRef](#)]
44. Jin, H.-G.; Wang, M.-F.; Hong, X.-J.; Yang, J.; Li, T.; Ou, Y.-J.; Zhao, L.-Z.; Cai, Y.-P. 2D pillar-chained lanthanide(III)-copper(I) metal–organic frameworks based on isonicotinate and in situ generated oxalate. *Inorg. Chem. Commun.* **2013**, *36*, 236–240. [[CrossRef](#)]
45. Vegas, V.G.; Maldonado, N.; Castillo, O.; Gómez-García, C.J.; Amo-Ochoa, P. Multifunctional coordination polymers based on copper with modified nucleobases, easily modulated in size and conductivity. *J. Inorg. Biochem.* **2019**, *200*, 110805–110814. [[CrossRef](#)]
46. Scano, A.; Mereu, E.; Cabras, V.; Mannias, G.; Garau, A.; Pilloni, M.; Orrù, G.; Scano, A.; Ennas, G. Green Preparation of Antimicrobial 1D-Coordination Polymers: [Zn(4,4'-bipy)Cl<sub>2</sub>]<sub>∞</sub> and [Zn(4,4'-bipy)2(OAc)2]<sub>∞</sub> by Ultrasonication of Zn(II) Salts and 4,4'-Bipyridine. *Molecules* **2022**, *27*, 6677. [[CrossRef](#)] [[PubMed](#)]
47. Trivedi, M.K.; Branton, A.; Trivedi, D.; Nayak, G.; Bairwa, K.; Jana, S. Spectroscopic Characterization of Disodium Hydrogen Orthophosphate and Sodium Nitrate after Biofield Treatment. *J. Chromatogr. Sep. Tech.* **2015**, *6*, 5. [[CrossRef](#)]
48. Nara, M.; Torii, H.; Tasumi, M. Correlation between the Vibrational Frequencies of the Carboxylate Group and the Types of Its Coordination to a Metal Ion: An ab Initio Molecular Orbital Study. *J. Phys. Chem.* **1996**, *100*, 19812–19817. [[CrossRef](#)]
49. Maldonado, N.; Vegas, V.G.; Halevi, O.; Martínez, J.I.; Lee, P.S.; Magdassi, S.; Wharmby, M.T.; Platero-Prats, A.E.; Moreno, C.; Zamora, F.; et al. 3D Printing of a Thermo- and Solvatochromic Composite Material Based on a Cu(II)–Thymine Coordination Polymer with Moisture Sensing Capabilities. *Adv. Funct. Mater.* **2019**, *29*, 1808424–1808435. [[CrossRef](#)]
50. Jimenez-Bescos, C.; Prewett, R. Monitoring IAQ and thermal comfort in a conservation area low energy retrofit. In Proceedings of the International Scientific Conference on Environmental and Climate Technologies (CONNECT), Riga, Latvia, 16–18 May 2018; Volume 147, pp. 195–201.
51. Silva, H.E.; Coelho, G.B.A.; Henriques, F.M.A. Climate monitoring in World Heritage List buildings with low-cost data loggers: The case of the Jerónimos Monastery in Lisbon (Portugal). *J. Build. Eng.* **2020**, *28*, 101029–1011046. [[CrossRef](#)]
52. Gu, H.-T.; Yang, Z.-H.; Fan, Z.; Jiang, W. Real-time in situ visualization of internal relative humidity in fluorescence embedded cement-based materials. *J. Cent. South Univ.* **2021**, *28*, 3790–3799. [[CrossRef](#)]

53. Qabbal, L.; Younsi, Z.; Naji, H. An indoor air quality and thermal comfort appraisal in a retrofitted university building via low-cost smart sensor. *Indoor Built Environ.* **2022**, *31*, 586–606. [[CrossRef](#)]
54. Castillo, O.; Alonso, J.; García-Couceiro, U.; Luque, A.; Román, P. A 2D polymer constructed through bridging oxalato and 4,4'-bipyridine ligands: Crystal structure and magnetic behavior of  $[\text{Cu}_3(\mu\text{-ox})_3(\mu\text{-4,4'-bpy})_2(4,4'\text{-bpy})_2]_n$ . *Inorg. Chem. Commun.* **2003**, *6*, 803–806. [[CrossRef](#)]
55. Mantasha, I.; Hussain, S.; Ahmad, M.; Shahid, M. Two dimensional (2D) molecular frameworks for rapid and selective adsorption of hazardous aromatic dyes from aqueous phase. *Sep. Purif. Technol.* **2020**, *238*, 116413. [[CrossRef](#)]
56. Huang, J.; Li, Y.-Z.; Sun, G.-C.; Dai, R.-B.; Li, Q.-X.; Wang, L.-F.; Xia, C.-G. Tetraaqua(5-fluorouracil-1-acetato-O)copper(II) tetrahydrate. *Acta Crystallogr. Sect. C* **2000**, *56*, 489–490. [[CrossRef](#)]

**Disclaimer/Publisher's Note:** The statements, opinions and data contained in all publications are solely those of the individual author(s) and contributor(s) and not of MDPI and/or the editor(s). MDPI and/or the editor(s) disclaim responsibility for any injury to people or property resulting from any ideas, methods, instructions or products referred to in the content.